A Full Field-of-View Self-Steering Beamformer for 5G mm-Wave Fiber-Wireless Mobile Fronthaul

Min-Yu Huang, *Student Member, IEEE*, You-Wei Chen, *Member, IEEE*, Peng-Chun Peng, *Member, IEEE*, Hua Wang, *Senior Member, IEEE*, and Gee-Kung Chang, *Fellow, IEEE, Fellow, OSA*

***Abstract*—The upcoming new radio access allows ultra-high data rate using millimeter-wave (mm-Wave) frequencies, while it normally suffers from large path loss. To compensate for path loss, phased arrays for both the transmitter and receiver are used. The 5G new radio (NR) three beam management process proceeds as follows: The transmitted beam is first swept in the downlink direction from the remote radio unit (RRU) to the user equipment (UE), and then the uplink beam is aligned to determine which beam direction has the best reception quality, and *vice versa*. However, this sequential beam management requires that the RX must be able to perform both beam detection and steering across all the reception angles. Moreover, due to the narrow beamwidth of the phased array operation, a "quantum leap" performance improvement of the receiver operating at mm-Wave is required. In this article, a self-steering array beamformer (SSA-BF) receiving system is proposed, which is composed of a home-designed IC package with zero DC power consumption and a 4-element antenna array. We first conduct the measurement without the antenna, and the SSA-BF receiver shows a significant array factor enhancement with negligible SNR degradation over full field-of-view (FoV) (incidence angle $= \pm 90°$), <3 ms fast beam alignment time, and it can support enhanced mobile data-rate up to 10 and 7.8 Gb/s with 20x100 MHz carrier aggregation OFDM in back-to-back and over 25-km fiber transmission, respectively. Moreover, a broadside 3-dB beamwidth $\pm 80°$ and broadband 17-36 GHz antenna is designed for the proposed SSA-BF receiver in a 5G fiber-wireless access. The SSA-BF receiving system with the 1×4 antenna array is designed at 28 GHz, and it shows the normalized array gain better than 3- and 6-dB degradation over broad FoV incidence $= \pm 68°$ and $\pm 85°$, respectively. Without any external tuning controls, the proposed SSA-BF achieves the state-of-the-art autonomous beamforming for 6 Gb/s 64-QAM signal over 50-cm wireless distance, achieving a substantial array factor improvement. To the best of authors' knowledge, this is the first demonstration of a high-speed switching SSA-BF receiver in a fiber-wireless integrated radio access as a true enabler for mm-Wave mobile fronthaul applications**

***Index Terms*—5G, beamforming, closed-loop, field-of-view (FoV), fiber-wireless network, millimeter-wave (mm-Wave), phased array.**

Manuscript received July 31, 2019; revised October 29, 2019 and November 20, 2019; accepted November 25, 2019. Date of publication November 29, 2019; date of current version March 17, 2020. *(Corresponding author: Min-Yu Huang.)*

M.-Y. Huang, Y.-W. Chen, H. Wang, and G.-K. Chang are with the School of Electrical and Computer Engineering, Georgia Institute of Technology, Atlanta, GA 30308 USA (e-mail: minyu@gatech.edu; yu-wei.chen@ece.gatech.edu; hua.wang@ece.gatech.edu; geekung.chang@ece.gatech.edu).

P.-C. Peng is with the Department of Electro-Optical Engineering, National Taipei University of Technology, Taipei 10608, Taiwan (e-mail: pcpeng@mail.ntut.edu.tw).

Color versions of one or more of the figures in this article are available online at https://ieeexplore.ieee.org.

Digital Object Identifier 10.1109/JLT.2019.2956667

I. Introduction

TO SUPPORT future wireless communication systems, such as 5G new radio (NR), orthogonal frequency division multiplexing (OFDM) using radio over fiber (RoF) technique in radio access network (RAN) [1] is adopted and standardized because its manageable signal processing resources enable flexible software defined RF operations and simplifies the remote radio units (RRU) architecture [3]–[12]. However, mm-Wave 5G-NR is susceptible to atmospheric attenuation such as water vapor and oxygen, suffering from higher wireless propagation loss. Therefore, in 5G communication network, RRUs can leverage large array sizes to substantially compensate the millimeter-wave (mm-Wave) link loss [3]–[38]; however, it results in a "pencil-like" beamwidth, which drastically complicates and poses challenges in the beam alignment for the transmitter and receiver. Moreover, unlike conventional static microwave beamforming in satellite communication, many future mm-Wave links are expected to operate in relatively "dynamic" environments, such as wireless AR/VR and machine-based communications, necessitating fast and precise beam-forming/-tracking to ensure high link reliability, enhanced data-rate and low latency, as shown in Fig. 1. Future dense deployment of mm-Wave small cells will result in a complex EM inter-cell interference and thus beam management is extremely important.

Beam management is composed of the following three step sequence [2], which are initial beam acquisition, transmitter beam refinement, and receiver beam refinement. The downlink is taken as an example in the following to elaborate the beam management process; while the uplink can follow the similar method in a reverse transmission direction. To initiate a data delivery for an idle user, the RRU first transmits and sweeps the beam to different directions via a synchronization signal burst set. Then, the UE will find the best-connected beam and feedback the information to the RRU. After the RRU knows the selected beam information, the second step will repeat the sweep process with a narrower beamwidth to UE and get a more accurate UE direction. To get the full beamforming gain, the receiver needs to refine and compute its receiving direction by reusing the beam information from the previous step. However, most receiver phase arrays have non-uniform array factor over scanning angles which can cause misjudgments in the beam alignment, for example, $\pm 30°$ and $\pm 90°$ incidences in a generic 4-element phase array antenna receiver. Therefore, to ensure UE feedback the accurate beam connection information in the first

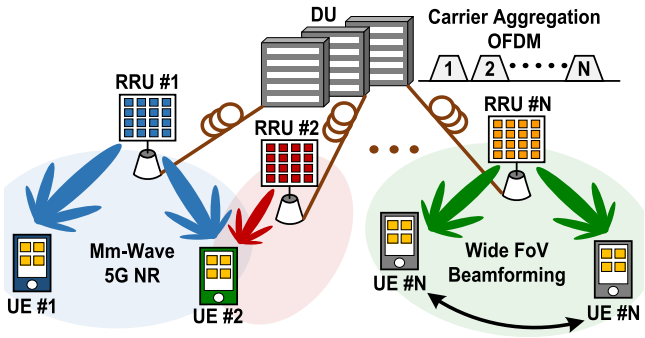

Fig. 1. Dynamic 5G fiber-wireless communication for uplink.

and second steps in future dynamic mobile environment, 5G-NR beam management requires an advanced receiver design with fast beam scanning, searching, forming, and computation over full reception angle.

Most existing beamforming systems in 5G fiber-wireless access are open-loop operations, which require extensive phase control signals [4]. Recently, a photonic-aid beamformer (BF) with higher operation bandwidth was reported based on array waveguide grating and dispersive fiber [5]; however, its feasibility is limited by its bulky size and thus it causes system stability issue due to environmental vibration, pressure, and temperature changes, which is problematic to precisely and stably align the beam toward the location of the UE. Photonic integrated circuit based phased array with 9.61 Gb/s has been demonstrated in [6]. However, the thermo-optical ring-resonator phase shifter is also sensitive to environmental temperature and difficult to achieve fast beamforming. Multiple calibrations are required to facilitate accurate beam-tracking, adding system complexity to future 5G ultra-reliable low-latency link.

To address these challenges in future dynamic mm-Wave mobile applications, we present a mm-Wave fiber-wireless integrated network with a broadband scalable full-FoV self-steering array beamformer (SSA-BF) over 25 km fiber link. The SSA-BF achieves calibration- and digital signal process (DSP)-free beamforming via zero-DC power consumption IC [39], [40] with a passive delay-locked-loop (DLL) phase domain negative feedback loops to cover 2-GHz wide bandwidth. A proof-of-concept experiment demonstrates that it can rapidly yet accurately align the desired signals with low-latency $<$3 ms beam-tracking and exhibits long-term system stability. The network has been demonstrated by probing-based measurement and it can achieve 20 $\times$ 100-MHz carrier aggregation OFDM with aggregating 10 Gb/s. In the over-the-air measurement, 6 Gb/s 64-QAM single-carrier signal is transmitted over 50-cm wireless distance for future high-speed and dynamic mm-Wave 5G fiber-wireless systems.

This paper is organized as follows. Section II presents the wideband full-FoV fiber-wireless SSA-BF system architecture. The operation principle and implementation details of the zero-DC SSA-BF IC as well as the wide-FoV antenna array design are demonstrated in Section III. Section IV shows the measurements and a performance comparison with various reported fiber-wireless systems.

II. Fiber-Wireless Self-Steering Beamforming

The proposed SSA-BF receiver system for a fiber-wireless network uplink includes mm-Wave front-end low noise amplifiers (LNAs), down-conversion mixers, zero-DC SSA beamforming IC package and electrical to optical converter (E/O converter). A proof-of-concept fiber-wireless system is designed at 28 GHz for mm-Wave 5G NR.

After down-conversion mixing, the IF signal is then sent to the home designed IC for conducting beamforming, including the angle of the arrival detection and beam alignment. The closed-loop IC consists of a passive power-aware phase detector, time-delay-based LC synthetic phase shifters, and resistive progressive feedback control voltage generation [40]. As shown in Fig. 2a, the negative feedback loop is realized by the passive phase detector with phase-to-voltage conversion G_1 and a DLL-based voltage-controlled phase shifter with voltage-to-phase conversion G_2 (Fig. 2b). In order to execute this close-loop beamforming operation, we have to ensure a large loop gain (LG) $= G_1G_2$ for autonomous operation over full-FoV and self-steering operation with zero DC power consumption [40].

In the first step of beamforming, when the incoming signals with an incident angle ϕ are injected into the receiver with a uniform $\lambda/2$ array (Fig. 2a), the middle two paths would induce an input progressive phase shift (IPPS) of $\theta_{in} = \pi \sin\phi$. Then, the successively power-aware phase detector would react to that phase deviation and feedback the compensation voltage V_{ctrl} for the phase shifters to generate θ_{FB}. Since it is a close-loop feedback manipulation, the feedback phase θ_{FB} would be subtracted from the input signal and thus reduce the phase difference in the adjacent paths. The residual output phase deviation θ_{res} can be expressed as [39], [40]:

$$\theta_{res} = \theta_{in} / (1 + G_1G_2) . \tag{1}$$

It is worth to note that θ_{res} is minimized as the total loop gain G_1G_2 is maximized, which implies a high accuracy for beam alignment of the received signal over a wide progressive phase shift range θ_{in}, i.e., wide FoV. The nonlinear conversion between the phase and voltage domain is further exploited in Section III.A to be extremely large even at end-fire incident angle (i.e., $\theta_{in} = \pm 180^\circ$ and $\phi = \pm 90^\circ$) [39], [40].

The SSA beamforming IC can be scalable for a large-scale phased array via generating a set of progressive feedback control voltages from the power-aware phase detector for the preceding phase shifters to align the entire array. For example, in Fig. 2a, $-3V_{ctrl}$, $-1V_{ctrl}$, $1V_{ctrl}$, and $3V_{ctrl}$ are generated for a uniform 1×4 array to compensate the input IPPS. After this autonomous phase detection and alignment, the N output channels are in-phase summed up to achieve a beamforming gain with *10logN* signal-to-noise ratio (SNR) and array factor enhancement. The SSA beamforming IC acts only on the signal power due to its nonlinear loop operation [40] and does not need any prior signal knowledge of angle of arrival information. Moreover, the all-passive design ensures its zero DC operation power, which is important for large-scaled phased arrays. To conduct the upstream signal transmission, the beamformed signal is then upconverted by an E/O converter and then sent to distributed unit

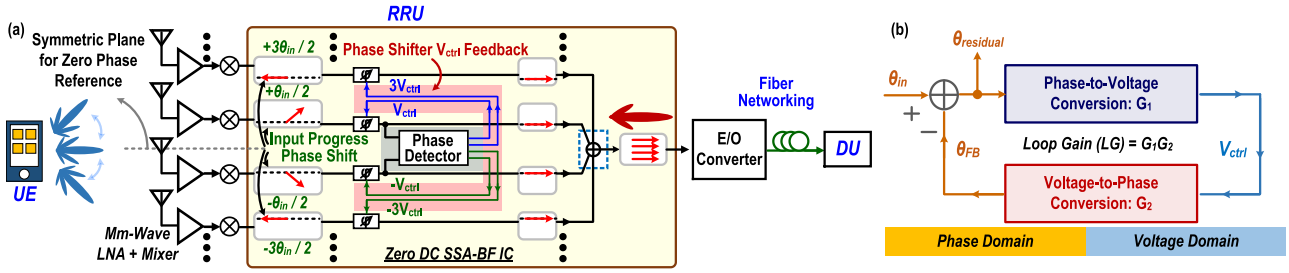

Fig. 2. (a) Operation principle of the full-FoV DLL-based negative feedback. (b) Conceptual diagram for scalable fiber-wireless SSA-BF.

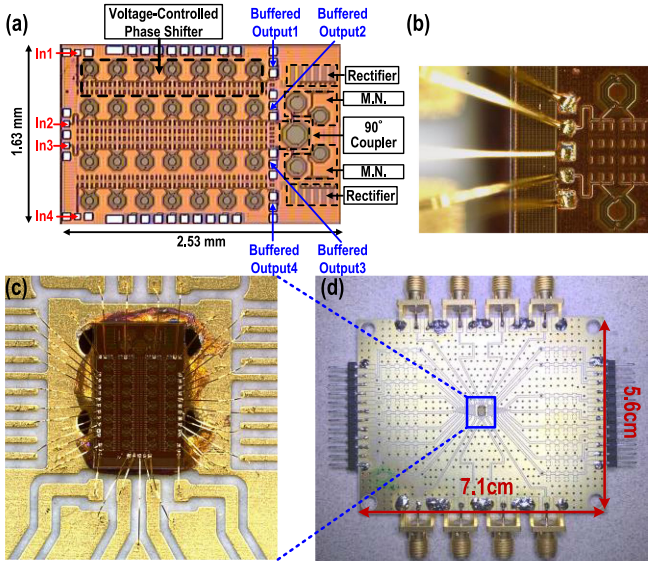

Fig. 3. (a) Chip microphotograph. (b) Zoom-in view, (c) complete wire-bonding view, and (d) full package of the zero-DC SSA-BF IC.

(DU) through the dedicated fiber links. Detailed system design and implementation are shown in the Section III.

III. System Implementation and Analysis

A. Operation of the Zero DC SSA Beamforming IC

To demonstrate the proposed mm-Wave fiber-wireless network with a full-FoV autonomous beamforming receiver, a proof-of-concept DLL-Like SSA beamforming IC is implemented in a 130 nm CMOS process with a size of 1.63 mm × 2.53 mm [40] and then packaged in low-loss FR4 PCB with an area of 5.6 cm × 7.1 cm to process the down-conversion 4–6 GHz IF signals (Fig. 3). The closed loop converts signals between two different domains, i.e., phase and voltage domains, and the loop gain is explored to be extremely large even though the circuitry is all-passive with zero DC power consumption [40].

1) Phase-to-Voltage Feedforward Conversion G_1: The phase-to-voltage feedforward convertor (phase detector) consists of a compact single-ended 90° coupler and a 7-stage Dickson voltage rectifier [39], [40]. The coupler is designed as a transformer-based poly-phased network [41]–[45] for a compact low-loss IQ generation [39], [40]. When the two signals in the adjacent path with $IPPS = \theta_{res}$ and with same amplitude A are injected to input and isolation ports of the 90° coupler, output signals at the through and coupled ports of the coupler are then followed by passive matching networks and the two 7-stage Dickson voltage rectifiers [40]. Assume that two matched rectifiers act as square-law devices, after the rectification, the differential DC voltage signal $V_{\rm ctrl}$ of the rectifier outputs can be expressed as [40]

$$V_{\rm ctrl} = 2\alpha\beta^2 A^2 \sin\theta_{res}, \tag{2}$$

where the factor β is the passive voltage amplification by the matching network and the coefficient α is rectification efficiency [40]. Note that the phase-to-voltage conversion is proportional to signal power A^2 and it is a power-aware phase detector without prior knowledge on angle of arrival. The differential DC outputs $V_{\rm ctrl}$ of the rectifiers are then sent to phase shifter to generate the feedback compensation phase $\theta_{\rm FB}$. The phase-to-voltage feedforward conversion is [40]

$$G_1 = V_{\rm ctrl}/\theta_{res} = 2\alpha\beta^2 A^2 \sin\theta_{res}/\theta_{res}. \tag{3}$$

2) Voltage-to-Phase Feedback Conversion G_2: To support wideband modulated signals for 5G NR, the zero DC SSA beamforming IC utilizes DLL-based delay lines for wideband phase shifting and signal processing. It is composed of a multi-section LC network as synthetic transmission lines for true-time delay [40]. The varactors in the multi-section LC network are controlled by the $V_{\rm ctrl}$ to generate corresponding feedback θ_{FB}, aligning adjacent channels and suppressing the θ_{res}.. The voltage-to-phase feedback conversion is [40]

$$G_2 = \theta_{FB}/V_{\rm ctrl}. \tag{4}$$

The overall loop gain G_1G_2 is exploited to be large even though it is composed of entirely of passive components and the large loop gain value is maintained over a wide FoV [15]–[19], [39], [40]. Moreover, the $V_{\rm ctrl}$ signals generated from the rectifier outputs of G_1 are further scaled via the resistive dividing loads [39], [40] to generate progressive $\pm V_{ctrl}, \pm 3V_{ctrl}$ for inner or outer path phase shifting (Fig. 2a), achieving a large-scale phased array. For this proof-of-concept design, since we only have one unit of phase shifter bonded in our testbed design, thus it only performs one beamforming toward one user. However, it could be scaled to the multi-user case if we integrate multiple phase shifters on our beamformer via a similar fashion.

3) Loop Analysis of Zero-DC SSA Beamforming IC: The overall closed loop of the zero-DC SSA beamforming IC is next analyzed. First, the output residual phase difference θ_{res} can be expressed as [40]

$$\begin{aligned}\theta_{res} &= \theta_{in}/\left(1+G_1G_2\right)\\ &= \pi\sin\phi/\left[1+(2\alpha\beta^2A^2\sin\theta_{res}/\theta_{res})G_2\right].\end{aligned} \quad (5)$$

Under different θ_{res}, the feedforward conversion gain G_1 varies during the feedback phase compensation and it is not a fixed value, showing the negative feedback loop is a nonlinear loop. It can be further modified as

$$\theta_{res} + k\,\sin\theta_{res} = \pi\sin\phi, \quad (6)$$

where $k = 2\alpha\beta^2A^2$, which is the loop gain value at incidence $\phi = 0°$. Moreover, *k* has a quadratic relationship to the incident signals amplitude, showing that the loop response is a function of the signal input power. Moreover, the transcendental equation (6) is further explored to achieve effective phase error reduction and high alignment accuracy. For a linear loop operation, the loop gain is normally peaking at broadside incident angle ($\phi = 0°$) and gradually decreasing when the signal is injected from end-fire region ($\phi = \pm 90°$). However, due to its nonlinear bifurcation behavior, the proposed power-aware closed loop can still maintain its large loop gain value across a large incident angle coverage and even at $\phi = \pm 90°$ or IPPS $\theta_{in} = \pm 180°$, showing the full-FoV operation as long as the *k* is $>>1$ [39], [40].

For the stand-alone SSA beamforming IC measurement, it can achieve wideband input matching ($S_{11} < -10$ dB) from 4 to 5.9 GHz to support wideband IF signals. With the feedback off, the zero-DC SSA beamforming IC behaves as a broadside phased array and forms an array factor null at IPPS $\theta_{in} = \pm 90°$ and $\pm 180°$, i.e., $\phi = \pm 30°$ and $\pm 90°$, in a uniform four-element array. With the feedback on, the measured normalized array factor of the SSA beamforming IC achieves significant array factor improvement (at least >25 dB) over full-FoV, i.e., IPPS from $-180°$ to $180°$ [39], [40]. Moreover, with a higher input power, the measured normalized array factor can be further improved over full-FoV because of its nonlinear operation [39], [40]. The array FoV is significantly expanded which cannot be realized via a linear feedback loop. Moreover, the proposed feedback operation is robust to corner variation and device mismatch and provide accurate phase shifting based on multiple chip sample measurements and Monte Carlo modeling simulations [40].

To achieve a larger LG and minimize the residual phase difference of the four paths even at end-fire incidence (IPPS $= \pm 180°$ or $\phi = \pm 90°$. Mm-Wave frontend LNAs and down-conversion mixers are applied before the SSA beamforming IC package to increase loop conversion gain and lower the system noise figure with better sensitivity. The IC package is wire bonded on the FR4 PCB and experimentally verified with Mm-Wave frontends as a Mm-Wave SSA-BF system. Overall nonlinear loop gain of the system is increased to achieve a flat normalized array factor over full-FoV, supporting the proposed SSA-BF to preserve self-steering operation even when receiving an end-fire signal (IPPS $= \pm 180°$ or $\phi = \pm 90°$). Moreover, the signals are operated in DLL-like loop, which can support wideband modulated signals through the following optical fiber as a proof-of-concept mm-Wave mobile fronthaul.

4) Experimental Verifications of SSA-BF With Fiber Link: The experimental setup of the proposed SSA-BF with fiber link is illustrated in Fig. 4a. We apply a 4-channels 16 GSa/s arbitrary waveform generator (AWG) to mimic the wireless signals with different incident angles for electrical phase shifting generation. The applied signals for this SSA-BF measurement are 1 Gbaud single carrier 64QAM, 10 and 20 100-MHz carrier aggregation of OFDM signal, which is generated via ordinary DSP [46], [47], including serial-to-parallel, inverse FFT, and cyclic prefix insertion. The output signals are firstly up-converted to 28 GHz for 5G-NR applications via a local oscillator (LO) and then pass through bandpass filters for sifting out the unwanted LO leakages. 4 LNAs with 2 dB noise figure from 26 to 40 GHz are employed to boost the input power up to 10 dBm before the proposed SSA-BF. It is worth bearing in mind that those wideband LNAs are applied for supporting multiple 5G-NR bands (especially at 28, 37, and 39 GHz), supporting future multi-standard communication and international roaming. After down-conversion to 5-GHz as center frequency, the 4 IF signals with corresponding IPPS are sent into the proposed SSA-BF, which chip photo of the SSA-BF are also shown in Fig. 4a.

After autonomous beamforming, the 4 in-phase output signals are directly summed up by a 4-to-1 power combiner and delivered to a direct modulation distributed feedback (DFB) laser with 1550.76 nm central wavelength and 5.5-dBm output power. After a 25-km fiber link, an optical attenuator and a10-GHz commercial photodetector (PD) are used to convert optical information to the electrical domain for testing received performance. After analog-to-digital conversion via a 20G GSa/s real-time oscilloscope (RTS), the received signals are then evaluated via their EVM, BER, SNR, and their corresponding constellation diagrams. Due to fully symmetric performance of the SSA-BF [40], a representative IPPS from 0° to 180° is used to characterize. The optical spectrum of 1 Gbaud 64QAM (6 Gb/s) single carrier after 25-km transmission is shown in Fig. 4b. Figure 4c demonstrates that the mm-Wave SSA-BF fiber fronthaul system can achieve low-latency response time <3 ms over full-FoV, supporting future dynamic 5G networks. The SSA-BF is also tested with a wideband modulated 1 Gbaud 64QAM (6 Gb/s) signal under different LG setting over full FoV and 25-km fiber link transmission. With a LG $= 30$, it remains similar SNR and shows clear constellations over full FoV in Fig. 4d. Fig. 4e exhibits the BER performance of the proposed full-FoV mm-Wave SSA-BF fiber fronthaul system with different IPPS. Again, the received performance is similar even when the IPPS is at end-fire 180°. The received sensitivities, defined as the received power at the FEC criterion, are -8 and -7 dBm for BtB and 25 km respectively. A 1 dB power penalty is measured due to the fiber dispersion. In Fig. 4f, over ten hours, stable EVM performance of 1 Gbaud 64QAM (6 Gb/s) single carrier is measured with 7.4% and 8.8% in BtB and 25-km scenario, showing that the SSA-BF fiber-wireless system still provide stable beamforming for the input wideband modulated Gb/s signal with a consistent EVM performance.

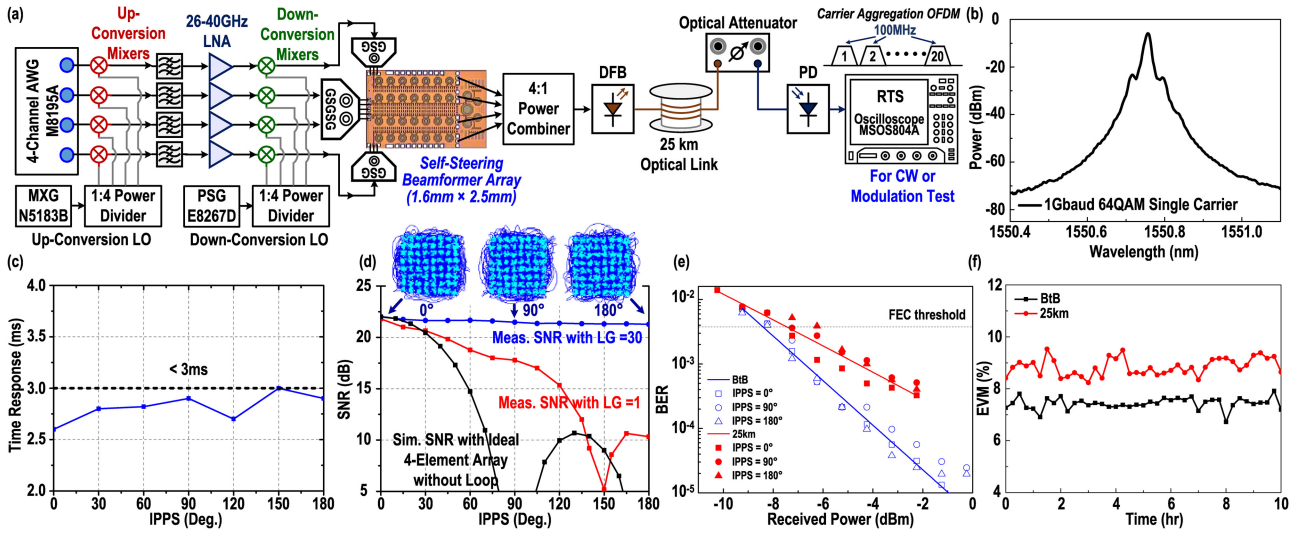

Fig. 4. (a) Experimental setup. (b) Optical spectrum of 1Gbaud 64QAM single carrier. (c) Response time of the SSA-BF mm-Wave SSA-BF fiber fronthaul system. (d) Received SNR versus IPPS. (e) The BER performance of 1Gbaud 64QAM single carrier with different IPPS in BtB and over 25-km fiber link. (f) Stability measurement of 1 Gbaud 64QAM single carrier over 10 hours.

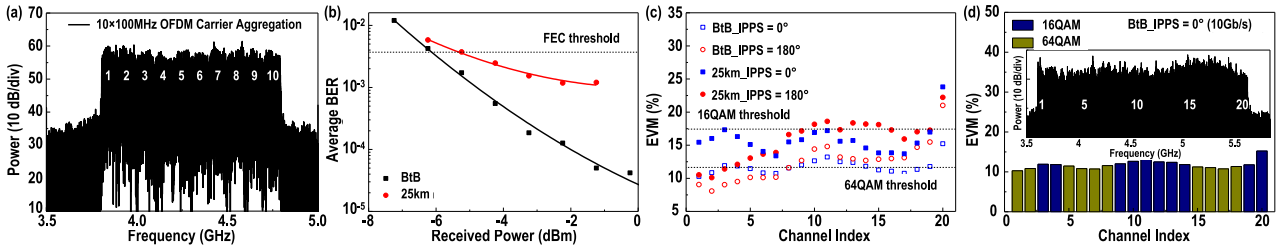

Fig. 5. (a) Electrical spectrum of 10 carrier aggregation of 100 MHz OFDM signals in BtB scheme. (b) Average BER performance of 10 carrier aggregation in BtB and over 25 km. (c) EVM performance of the 20 x100 MHz carrier aggregation OFDM as IPPS = 0° and 180° IPPS. (d) Upper inset, 20 x100 MHz signal; lower inset, maximum EVM in achievable QAM level BtB scheme with IPPS = 0° (64QAM × 10, 16QAM × 10).

Fig. 5a shows the electrical spectra of 10 carrier aggregation of 100 MHz OFDM bands with an accommodated 1 GHz bandwidth. Each of them has similar SNR and the average BER performance shows the received sensitivity (FEC threshold BER $= 3.8 \times 10^{-3}$) is -6 dBm of the BtB scheme and -5 dBm after the 25 km link respectively in Fig. 5b. Compared to the 1 Gbaud 64QAM (6 Gb/s) single carrier, the performance of the OFDM signals is slightly degraded due to higher PAPR and lower SNR under the constrained linearity of the front-end LNAs. To further enhance mobile data capacity of the proposed mm-Wave SSA-BF fiber fronthaul system, 20 carrier aggregation OFDM signals with total 2 GHz bandwidth are applied and are successfully demodulated. By applying different QAM levels to different OFDM bands, we can achieve raw data rate under FEC threshold to support 10 Gb/s and 9.4 Gb/s in BtB scheme as well as 7.8 Gb/s and 7.4 Gb/s over 25-km fiber transmission with 0- and 180-degree IPPS respectively. The corresponding QAM level among each OFDM bands and electrical spectrum in the BtB scheme with 0-degree IPPS is also presented in Fig. 5d. With 7% FEC overhead, 1/32 CP length, 10% training symbols, and 10% signal guard band, we can achieve a net data rate of 7.3 Gb/s in BtB and 5.7 Gb/s for over 25 km, showing the mm-Wave SSA-BF fiber fronthaul system with full FoV and self-tracking abilities for future mm-Wave enhanced mobile services. The measurements in Section III-A.4 are based on electrical phase shifting and it shows a flat array factor enhancement with negligible SNR degradation over full-FoV and supports enhanced mobile data-rate carrier aggregation OFDM over 25-km fiber transmission without considering FoV coverage of the antenna. However, in the practical scenarios, the FoV coverage of the entire fiber-wireless SSA-BF system is also limited by the antenna design. In following section III-B, a proof-of-concept broadband wide-FoV antenna is presented.

B. Broadband Wide-FoV Antenna Design

To extend FoV and broadband coverage, a bow-tie dipole antenna fabricated on two-layer Rogers RO40350 with 10mil height and 1oz cooper thickness is proposed to support a mm-Wave low-loss antenna design (Fig. 6). The top signal layer is first designed via differential feeding lines with differential impedance $\sim$100 Ω. One of feeding line is meandered to create out-of-phase 180° difference and they are then combined as one input single-end 50 Ω feeding transmission line with passive loss

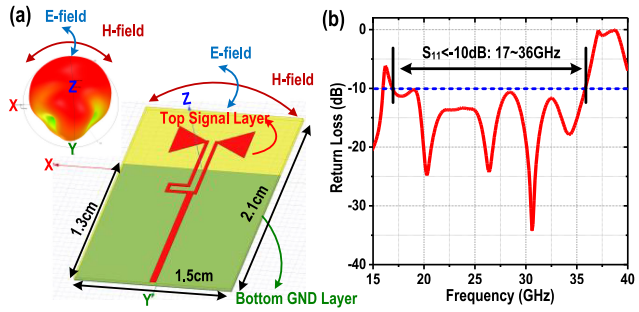

Fig. 6. (a) 3D EM HFSS model and radiation pattern of the proposed bow-tie antenna. (b) Measured input matching S_{11} of the antenna.

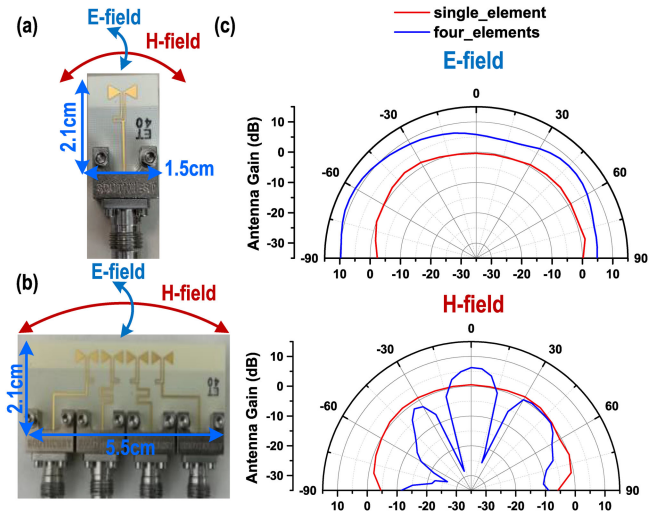

Fig. 7. Fabricated (a) single-element and (b) four-element antenna design. (c) Measured E- and H- field performance of the single-element and four-element antenna designs at 28 GHz.

1.5 dB at 28 GHz (Fig. 6a). On the other hand, the bottom copper layer is served as PEC plane and designed as a finite ground to create extremely broadside FoV coverage and multi-resonance broadband frequency response. The 3D EM simulations of the broadside radiation at 28 GHz and the antenna are shown in Fig. 6a with ground size of 1.5 cm $\times$ 1.3 cm and entire antenna area of 1.5 cm $\times$ 2.1 cm. Measured input matching $S_{11} < -10$ dB is from 17 GHz to 36 GHz, supporting wideband multi-5G standard communication (Fig. 6b).

Then, the single-element antenna and the four-element antenna array are connected with southwest connectors for far-field radiation test (Fig. 7). Four meandering transmission line traces in the four-element antenna array are applied for equal phase distribution for the four inputs and the area of the array is 2.1 cm $\times$ 5.5 cm (Fig. 7b). In the single-element antenna, the antenna gain patterns are measured with a peak antenna gain 2 dBi and wide 3-dB beamwidth FoV $= \pm 80°$ coverage (total 160° incidence) on both E- and H-field, showing a state-of-the-art broadside performance [34], [35]. Note that the overall array gain pattern of the fiber-wireless system is a product of the antenna gain of each element and the beamforming array factor. Since the proposed SSA-BF generates near-ideal autonomous beamforming array factor over full-FoV, the far-field array gain pattern measurement in Section IV of the entire fiber-wireless SSA-BF system is limited by the FoV of the antenna.

The far-field performance of four-element antenna array is then measured with an in-phase 4-to-1 power combiner without any phase tuning. Due to the IPPS of the four-element antenna arrays in H-field, the measured array gain peaks with $10 \times \log 4 = 6$ dB array factor enhancement compared to the single-element antenna and the 3-dB beamwidth FoV coverage is largely decreased from 160° to 20° (Fig. 7c). With the proposed SSA-BF, the peak of the array gain real-time autonomously tracks and beamforms to the incoming signal over full-FoV with significant array factor improvement in the proposed fiber-wireless SSA-BF system (Section IV).

IV. Far-Field Experimental Results

Fig. 8a exhibits the experimental setup of far-field over-the-air measurement over 50 cm mm-Wave wireless transmission and 25 km fiber link. The 1Gbaud single carrier signal is generated via a 64 GSa/s AWG, and then up-converted to 28 GHz by external mm-Wave mixers. A horn antenna with 25 dBi Gain is then employed for wireless signal delivery (Fig. 8a). The wireless transmission distance is conducted under the far-field criteria, which is expressed as

$$R_f = 2D^2/\lambda, \tag{7}$$

where R_f, D, and λ are the radiating far-field distance, antenna diameter, and the RF signal wavelength respectively. To operate the wireless link at 28 GHz, R_f needs to be >42 cm and the received signal could be approximately as plane waves with the progressive phase shifts across adjacent channels. In order to sweep full-FoV coverage in wireless measurement, an antenna arm is required but the distance from antenna arm to antenna front-end can only be maximized to 50 cm due to our existing antenna chamber room limitation. After the four-element antenna array, the received signals are firstly amplified via the wideband LNAs with 25 dB gain, and then frequency down-converted via 23-GHz LO mixers. The beamformer is operated at 5-GHz IF frequency to accommodate IF signal bandwidth and practical IC package design issue, which is especially easy for accurate phase matching, and lower propagation loss at RF frequency rather than at mm-Wave frequency. After an initial one-time calibration between the antenna array and the SSA-BF system for phase and amplitude correction, measured array patterns of four-element fiber-wireless system over full FoV with/without the proposed SSA-BF are shown in Fig. 8b.

The available reception angle of the proposed beamformer is evaluated via a 28-GHz single-tone mm-Wave source as shown in Fig. 8b. Without employing the proposed beamformer, power fading (< -30 dBc), i.e., array factor null, incurs as the incident angle are near $-30°$ and 30°. The result is similar as an ideal static four-element array factor without self-steering. On the other hand, with the proposed SSA-BF, the measured normalized array gain pattern better than 3-dB and 6-dB degradation is largely improved to cover wide FoV incidence $= 136°$ and 170°,

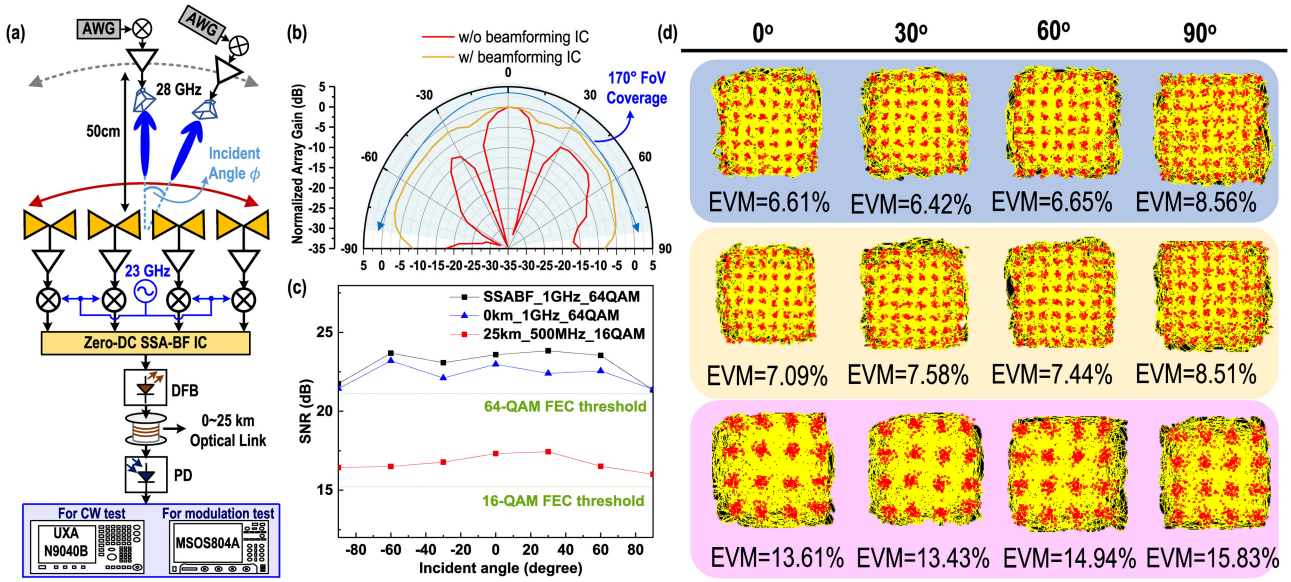

Fig. 8. (a) Far-field experimental setup for the proposed SSA-BF fiber-wireless system. (b) Far-field normalized antenna array gain pattern versus with incident angles. (c) Measured far-field SNR of SSA-BF only, SSA-BF with BtB fiber link, and SSA-BF with 25 km fiber link over full FoV. (d) Measured constellations and EVMs over full FoV in different case scenarios of SSA-BF only testing; b2b and 25-km transmission following the order from the top to bottom.

TABLE I
COMPARISON WITH STATE-OF-THE-ART ANTENNA, OPTICAL BEAMFORMER, AND FIBER-WIRELESS SYSTEM

	M. Michele Sisto *OFC'10*	T. Mengual. *OFC'08*	C. G. H. RoeloffzenJ *OFC'15*	N.M. Tessema *MPW'17*	H. Lu, *OFC'18*	A.M. Trinidad *OFC'18*	K. Furuya *IEICE'17*	V. C. Duarte *OFC'18*	This Work
Element No.	4	8	16	4	4	4	2×4	4	4
Frequency (GHz)	N/A	7.5-8.5	11.72	20	22-25	20	60	28	28
Topology	Thermal or stretching controlled FBG	Optical TDD with spatial light modulator	Thermal controlled phase shifter	Thermal controlled phase shifter	Optical comb lines with SCM	single optical ring resonator for phase shifting	Optical variable delay lines	True time delay phase tuner and DSP	True time DLL with all-passive nonlinear loop
Beamforming	Open-Loop	Open-Loop	Open-Loop	Open-Loop	Open-Loop	Open-Loop	Open-Loop	Closed-loop	Closed-loop
Electrical Phase Shifting Incident FoV Coverage	-60°~30°	N/A	N/A	N/A	-48°~35°	N/A	N/A	N/A	Full-FoV -90°~90°
Radio Over Fiber (Distance)	N/A	Yes (N/A)	N/A	N/A	N/A	Yes (85 cm)	Yes (35 cm)	N/A	Yes (50 cm)
Antenna Array Far-Field Incident FoV Coverage	N/A	20°	N/A	N/A	N/A	45°	40°	N/A	3-dB AG Degradation*: -68°~68° 6-dB AG Degradation*: -85°~85°
Response Time	N/A	N/A	N/A	N/A	N/A	N/A	N/A	~10s	< 0.003s
Modulation Scheme	N/A	N/A	N/A	32-QAM	16-QAM	16-QAM	QPSK	QPSK	64-QAM
EVM	N/A	N/A	N/A	9.61 Gb/s	8 Gb/s	2.8 Gb/s	3.5 Gb/s	1 Gb/s	6 Gb/s: 64-QAM 10.08 Gb/s: bit-loading

AG Degradation* : Normalized array gain degradation.

respectively, showing that the proposed SSA-BF effectively and autonomously traces the incident signal and beamforms the summing signal towards the desired direction over the extreme FoV.

Then, the modulated beamforming signal from the proposed SSA-BF is launched into a 10 GHz direct-modulated laser as electrical-optical conversion for optical signal delivery over 25 km fiber link. Since the input power is a crucial parameter, we also conducted power matching for each channel before each signal enters the beamformer. The single channel input power of the first-stage wideband LNAs is −38 dBm. After the proposed beamformer, the output signal for the successive DFB is −3 dBm. Then, a commercial 10-GHz PD is employed to conduct the opto-electrical down conversion with −0.6 dBm received optical power. After the signal is analog-to-digital converted via an 8-GHz, 20 GSa/s RTS, it is decoded by a Keysight Vector Signal Analyzer with 0.035 filter roll-off and FIR equalizer (Fig. 8a). Fig. 8c shows the received SNR with over-the-air measurement coverage over the full FoV incidence. The black curve represents the SSA-BF only testing without the optical

components and it shows the best received performance with stabile SNR of near 24 dB in most of the cases, and a 3-dB SNR drop at the end-fire angles (incidence $= \pm 90°$). As the beamformed signal passing through the optical channel, additional noises and signal losses slightly degrades the received SNR as the blue curve in Fig. 8c. Note that the SNR at the end-fire angle is mainly dominated by the SSA-BF loop gain performance and the limited antenna FoV, and the measured corresponding demodulated EVM performance are similar at end-fire angles in both SSA-BF only testing and BtB transmission scheme. While, after 25-km fiber link, the received SNR is further reduced by about 5 dB and thus the available QAM level is declined to 16 QAM, which can be improved by applying a PD with a higher received sensitivity or adopting IF LNAs before the RTS. *To the best of our knowledge, this is a first-ever fiber-wireless SSA-BF system to achieve the state-of-the-art wideband 6 Gb/s 64-QAM single carrier with EVM above the FEC threshold in an optical system over full-FoV* $\pm 90°$ *incidence.*

V. Conclusion

This paper presents the first fiber-wireless system that achieves autonomous beamforming on unknown angle of arrival signals, 64-QAM multi-Gb/s wideband modulated signal beamforming, extreme wide FoV coverage for radio over fiber, and fast response time <3 ms, supporting future emerging mm-Wave 5G mobile fronthaul application.

References

[1] G. K. Chang *et al.*, "Grand challenges of fiber wireless convergence for 5G mobile data communications," in *Proc. Optoelectronics Commun. Conf.*, 2018, pp. 1–2.

[2] A. Ghosh, "5G New Radio (NR): Physical layer overview and performance," in *Proc. IEEE Commun. Theory Workshop*, May 2018, pp. 1–38.

[3] A. M. Trinidad *et al.*, "Optical beamformer for K-band smart antenna systems," in *Proc. Opt. Fiber Commun. Conf.*, 2018, Paper M4J.2.

[4] H. Lu *et al.*, "mmWave beamforming using photonic signal processing for future 5G mobile systems," in *Proc. Opt. Fiber Commun. Conf.*, 2018, Paper M4J.3.

[5] K. Furuya *et al.*, "60 GHz-band photonic-integrated array-antenna and module for radio-over-fiber-based beam forming," *IEICE Trans. Commun.*, vol. E100-B, no. 10, pp. 1717–1725, 2017.

[6] N. M. Tessema *et al.*, "A photonic-assisted beamformer for K-band RF antenna arrays," in *Proc. Int. Topical Meeting Microw. Photon.*, 2017, pp. 1–4.

[7] C. G. H. Roeloffzen *et al.*, "Integrated optical beamformers," in *Proc. Opt. Fiber Commun. Conf.*, 2015, Paper Tu3F.4.

[8] G.-K. Chang and Y.-W. Chen, "Key fiber wireless integrated radio access technologies for 5G and beyond," in *Proc. Optoelectronics Commun. Conf.*, 2019, pp. 1–3.

[9] T. Mengual *et al.*, "Optical beamforming network with multibeam capability based on a spatial light modulator," in *Proc. Opt. Fiber Commun. Conf.*, 2008, Paper JThA71.

[10] G.-K. Chang and P.-C. Peng, "Grand challenges of fiber wireless convergence for 5G mobile data communications," in *Proc. Optoelectronics Commun. Conf.*, 2018, pp. 1–2.

[11] M. M. Sisto *et al.*, "Optical phase and amplitude control for beamforming with cascades of Gires-Tournois Bragg grating filters," in *Proc. Opt. Fiber Commun. Conf.*, 2010, Paper OThF3.

[12] V. C. Duarte *et al.*, "Integrated photonic true-time delay beamformer for a Ka-band phased array antenna receiver," in *Proc. Opt. Fiber Commun. Conf.*, 2018, Paper M2G.5.

[13] T. Chi, H. Wang, M. Huang, F. Dai, and H. Wang, "A bidirectional lens-free digital-bits-in/-out 0.57 mm2 terahertz nano-radio in CMOS with 49.3 mW peak power consumption supporting 50 cm Internet-of-Things communication," in *Proc. IEEE Custom Integr. Circuits Conf.*, May 2017, pp. 1–4.

[14] W. Roh *et al.*, "Millimeter-wave beamforming as an enabling technology for 5G cellular communications: Theoretical feasibility and prototype results," *IEEE Commun. Mag.*, vol. 52, no. 2, pp. 106–113, Feb. 2014.

[15] M.-Y. Huang, T. Chi, F. Wang, T.-W. Li, and H. Wang, "A 23-to-30 GHz hybrid beamforming MIMO receiver array with closed-loop multistage front-end beamformers for full-FoV dynamic and autonomous unknown signal tracking and blocker rejection," in *IEEE Int. Solid–State Circuits Conf. Dig. Tech. Papers*, Feb. 2018, pp. 68–70.

[16] Y. Tang *et al.*, "A 4-channel beamformer for 9-Gb/s MMW 5G fixed-wireless access over 25-km SMF with bit-loading OFDM," in *Proc. Opt. Fiber Commun. Conf.*, 2019, Paper W3J.7.

[17] M.-Y. Huang, T. Chi, F. Wang, T.-W. Li, and H. Wang, "A full-FoV autonomous hybrid beamformer array with unknown blockers rejection and signals tracking for low-latency 5G Mm-wave links," *IEEE Trans. Microw. Theory Techn.*, vol. 67, no. 7, pp. 2964–2974, Apr. 2019.

[18] S. Li *et al.*, "An E-band high-linearity antenna-LNA frontend with 4.8 dB NF and 2.2 dBm IIP3 exploiting multi-feed on-antenna noise-canceling and Gm-boosting," in *IEEE Int. Solid-State Circuits Conf. Dig. Tech. Papers*, Feb. 2020.

[19] M. Huang and H. Wang, "A 27–41 GHz MIMO receiver with n-input-n-output using scalable cascadable autonomous array-based high-order spatial filters for instinctual full-FoV multi-blocker/signal management," in *IEEE Int. Solid-State Circuits Conf. Dig. Tech. Papers*, Feb. 2019, pp. 346–348.

[20] N. S. Mannem, M. Huang, T. Huang, S. Li, and H. Wang, "A reconfigurable series/parallel quadrature coupler Doherty PA in CMOS-SOI with VSWR resilient linearity and back-off PAE for 5G MIMO arrays," *IEEE Int. Solid-State Circuits Conf. Dig. Tech. Papers*, Feb. 2020.

[21] T. Chi, F. Wang, S. Li, M. Huang, J. S. Park, and H. Wang, "A 60 GHz on-chip linear radiator with single-element 27.9 dBm PSAT and 33.1 dBm peak EIRP using multifeed antenna for direct on-antenna power combining," in *Proc. IEEE Int. Solid-State Circuits Conf.*, Feb. 2017, pp. 296–297.

[22] S. Li, M. Huang, D. Jung, T. Huang, and H. Wang, "A 28 GHz current-mode inverse-outphasing transmitter achieving 40%/31% PA efficiency at PSAT/6 dB PBO and supporting 15 Gbit/s 64QAM for 5G communication," in *IEEE Int. Solid-State Circuits Conf. Dig. Tech. Papers*, Feb. 2020.

[23] F. Wang, T.-W. Li, and H. Wang, "A highly linear super-resolution mixed-signal Doherty power amplifier for high-efficiency mm-Wave 5G multi-Gb/s communications," in *IEEE Int. Solid-State Circuits Conf. Dig. Tech. Papers*, Feb. 2019, pp. 88–90.

[24] T. Li, M. Huang, and H. Wang., "A continuous-mode harmonically tuned 19- to-29.5 GHz ultra-linear PA supporting 18 Gb/s at 18.4% modulation PAE and 43.5% peak PAE," in *Proc. IEEE Int. Solid-State Circuits Conf.*, Feb. 2018, pp. 410–412.

[25] H. Wang *et al.*, "Towards energy-efficient 5G mm-wave links: Exploiting broadband mm-wave Doherty power amplifier and multi-feed antenna with direct on-antenna power combining," in *Proc. IEEE Bipolar/BiCMOS Circuits Technol. Meeting*, Sep. 2017, pp. 30–37.

[26] M. Huang, T. Chi, F. Wang, S. Li, T. Huang, and H. Wang, "A 24.5-43.5 GHz compact RX with calibration-Free 32–56 dB full-frequency instantaneously wideband image rejection supporting multi-Gb/s 64-QAM/256-QAM for multi-band 5G massive MIMO," in *Proc. IEEE RF Integr. Circuits Symp.*, Jun. 2019, pp. 275–278.

[27] T. Chi, M. Huang, S. Li, and H. Wang, "A packaged 90-to-300 GHz transmitter and 115-to-325 GHz coherent receiver in CMOS for full-band continuous-wave mm-wave hyperspectral imaging," in *Proc. IEEE Int. Solid-State Circuits Conf.*, Feb. 2017, pp. 304–305.

[28] K. Dasgupta *et al.*, "A 60-GHz transceiver and baseband with polarization MIMO in 28-nm CMOS," *IEEE J. Solid-State Circuits*, vol. 53, no. 12, pp. 3613–3627, Dec. 2018.

[29] M. Huang and H. Wang, "A mm-Wave wideband MIMO RX with instinctual array-based blocker/signal management for ultra-low-latency communication," *IEEE J. Solid-State Circuits*, vol. 54, no. 12, pp. 3553–3564, Dec. 2019.

[30] S. Li *et al.*, "A buffer-less wideband frequency doubler in 45 nm CMOS-SOI with transistor multi-port waveform shaping achieving 25% drain efficiency and 46-89 GHz instantaneous bandwidth," *IEEE Solid-State Circuits Lett.*, vol. 2, no. 4, pp. 25–28, Apr. 2019.

[31] T. Li, M. Huang, and H. Wang., "Millimeter-wave continuous-mode power amplifier for 5G MIMO applications," *IEEE Trans. Microw. Theory Techn.*, vol. 67, no. 7, pp. 3088–3098, Apr. 2019

[32] S. Li, T. Chi, and H. Wang, "A millimeter-wave dual-feed square loop antenna for 5G communications," *IEEE Trans. Antennas Propag.*, vol. 65, no. 12, pp. 6317–6328, Dec. 2017.

[33] S. Mondal and J. Paramesh, "A reconfigurable 28-/37-GHz MMSE-adaptive hybrid-beamforming receiver for carrier aggregation and multi-standard MIMO communication," *IEEE J. Solid–State Circuits*, vol. 54, no. 5, pp. 1391–1406, Jan. 2019.

[34] S. Li, T. Chi, J. Park, and H. Wang, "A multi-feed antenna for antenna-level power combining," in *Proc. IEEE Int. Symp. Antennas Propag.*, Jun. 2016, pp. 1589–1590.

[35] H. Ullah, F. A. Tahir, and Z. Ahmad, "A dual-band hexagon monopole antenna for 28 and 38 GHz millimeter-wave communications," in *Proc. IEEE Int. Symp. Antennas Propag.*, Jul. 2018, pp. 1215–1216.

[36] J. Pang *et al.*, "A 28-GHz CMOS phased-array transceiver based on LO phase-shifting architecture with gain invariant phase tuning for 5G new radio," *IEEE J. Solid-State Circuits*, vol. 54, no. 5, pp. 1228–1242, Mar. 2019.

[37] S. Li, T. Chi, J. Park, W. Tanveer, H. Wang, and J. Papapolymerou, "A fully packaged D-band MIMO transmitter using high-density flip-chip interconnects on a flexible LCP substrate," in *Proc. IEEE Int. Microw. Symp.*, May 2016, pp. 1–4.

[38] B. Sadhu *et al.*, "A 28-GHz 32-element TRX phased-array IC with concurrent dual-polarized operation and orthogonal phase and gain control for 5G communications," *IEEE J. Solid-State Circuits*, vol. 52, no. 12, pp. 3373–3391, Dec. 2017.

[39] M. Huang, T. Chi, and H. Wang, "A 5 GHz all-passive negative feedback network for RF front-end self-steering beamforming with zero DC power consumption," in *Proc. IEEE RF Integr. Circuits Symp.*, May 2016, pp. 91–94.

[40] M. Huang, T. Chi, F. Wang, and H. Wang, "An all-passive negative feedback network for broadband and wide field-of-view self-steering beam-forming with Zero DC power consumption," *IEEE J. Solid-State Circuits*, vol. 52, no. 5, pp. 1260–1273, May 2017.

[41] S. Lee, M. Huang, Y. Youn, and H. Wang, "A 15–55 GHz low-loss ultra-compact folded inductor-based multi-section Wilkinson power divider for multi-band 5G applications," in *Proc. IEEE Int. Microw. Symp.*, Jun. 2019, pp. 432–435.

[42] M. Huang and H. Wang, "An ultra-compact folded inductor-based mm-Wave rat-race coupler in CMOS," in *Proc. IEEE Int. Microw. Symp.*, May 2016, pp. 1–4.

[43] M. Huang, "Ultra-compact concurrent multi-directional beamforming receiving network for high-efficiency wireless power transfer (WPT)," M.S. thesis, Dept. Elect. Comput. Eng., Georgia Tech, Atlanta, GA, USA, Jan. 2019. [Online]. Available: http://hdl.handle.net/1853/60829

[44] E. Garay, M. Huang, and H. Wang, "A cascaded self-similar rat-race hybrid coupler architecture and its compact fully integrated Ka-band implementation," in *Proc. IEEE Int. Microw. Symp.*, Jun. 2018, pp. 79–82.

[45] M. Huang, T. Huang, M. Swaminathan, and H. Wang, "Concurrent multi-directional beamforming receiving network for full-FoV high-efficiency wireless power transfer," in *Proc. IEEE Int. Microw. Symp.*, Jun. 2019, pp. 1511–1514.

[46] Y.-W. Chen *et al.*, "RF power fading mitigation for an IMDD multicarrier LR-PON," *Opt. Exp.*, vol. 24, no. 14, pp. 19311–19321, 2016.

[47] Y.-W. Chen *et al.*, "A reliable OFDM based MMW mobile fronthaul with DSP-aided sub-band spreading and time-confined windowing," *J. Lightw. Technol.*, vol. 37, no. 13, pp. 3236–3243, Jul. 2019.